

RSC Advances



This is an *Accepted Manuscript*, which has been through the Royal Society of Chemistry peer review process and has been accepted for publication.

Accepted Manuscripts are published online shortly after acceptance, before technical editing, formatting and proof reading. Using this free service, authors can make their results available to the community, in citable form, before we publish the edited article. This *Accepted Manuscript* will be replaced by the edited, formatted and paginated article as soon as this is available.

You can find more information about *Accepted Manuscripts* in the [Information for Authors](#).

Please note that technical editing may introduce minor changes to the text and/or graphics, which may alter content. The journal's standard [Terms & Conditions](#) and the [Ethical guidelines](#) still apply. In no event shall the Royal Society of Chemistry be held responsible for any errors or omissions in this *Accepted Manuscript* or any consequences arising from the use of any information it contains.

ARTICLE

Effects of Alkanethiols Chain Length on Synthesis of Cu_{2-x}S Nanocrystals: Phase, Morphology, Plasmonic Properties and Electrical Conductivity

Cite this: DOI: 10.1039/x0xx00000x

Received
Accepted

DOI: 10.1039/x0xx00000x

www.rsc.org/Xu Li,^{a,b} Aiwei Tang,^{a*} Li Guan,^{a,b} Haihang Ye,^a Yanbing Hou,^a Guoyi Dong,^b Zhiping Yang,^b and Feng Teng^{a,b}

Cu_{2-x}S nanocrystals with different morphologies and crystal phases have been synthesized by using a simple one-pot and phosphine-free colloidal method, in which different alkanethiols ($\text{C}_n\text{H}_{2n+1}\text{SH}$, $n=8, 12, 18$) have been selected as sulfur sources and capping ligands. The crystal phase can be transformed from monoclinic $\text{Cu}_{1.94}\text{S}$ to tetragonal $\text{Cu}_{1.81}\text{S}$ by varying the alkyl chain length of alkanethiols, and the morphology changes from nanospheres to nanodisks during the phase transformation. Strong localized surface plasmon resonance (LSPR) absorbance in the near-infrared (NIR) region has been observed in these Cu_{2-x}S nanocrystals, which originates from excess holes in the valence band due to copper deficiencies. The alkyl chain length of alkanethiols plays an important role in the crystal phase, morphology and plasmonic properties of the as-obtained Cu_{2-x}S nanocrystals.

Introduction

In the past few decades, more and more attention has been paid to semiconductor nanocrystals (NCs) due to their unique size-dependent properties as well as potential applications in optoelectronic devices and biological fields¹⁻³. However, the existing semiconductor NCs mainly focus on II-VI and IV-VI semiconductors, which often contain highly toxic elements, such as cadmium (Cd) and lead (Pb), *etc.* With the urgent demanding of environmental protection, it is necessary to exploit a series of environmental-benign semiconductor NCs. To date, different types of semiconductor NCs have been developed, in which copper-based NCs have attracted enormous interests⁴⁻⁸. Among them, copper sulfide (Cu_{2-x}S) ($x=0-1$) is a well-known *p*-type semiconductor and its band gaps varies with the stoichiometry (value of x) ranging from Cu-rich Cu_2S (chalcocite) to CuS (covellite), which holds great promise in photo thermal therapy, thermo electronics, solar cells and Li-ion battery⁹⁻¹². Therefore, the synthesis of Cu_{2-x}S NCs with different composition and morphologies has become another research spot.

So far, several colloidal synthesis methods have been developed to prepare Cu_{2-x}S NCs with controlled Cu stoichiometry, such as hot-injection method¹³, hydro- or solvothermal approach^{14, 15}, solventless thermolytic method¹⁶, cation-exchange reaction and water-oil interface confined method^{17, 18}, and so on. For example, Korgel et al synthesized Cu_2S nanodisks (NDs) through a solventless thermolytic approach by using sodium octanoate as both the phase transfer catalyst and the capping ligand, and they found that the as-

obtained Cu_2S NDs can self-assemble into ribbons of stacked platelets¹⁹. Kolny-Olesiak et al prepared Cu_2S nanorods (NRs) by using hot-injection approach, in which the tert-dodecanethiol (*t*-DDT) was used as sulfur sources. The length of the as-obtained NRs can be tailored from 10 to 100 nm by adjusting the nucleation temperature and copper monomer concentration²⁰. Very recently, Plass et al observed the crystal structure and stoichiometry of Cu_{2-x}S can be effectively controlled by varying the ratio of 1-dodecanethiol (1-DDT) to oleic acid²¹. We have developed one-pot colloidal approach to prepare Cu_2S NCs by using 1-DDT as sulfur sources and oleylamine (OLA) as a coordinating agent, and the morphology of the as-obtained products can be changed from nanospheres (NSs) to NDs by elevating the reaction temperature. Also the as-obtained products have a high tendency to self-assemble into highly ordered nanoarrays²². Different from Cu_2S , $\text{Cu}_{1.94}\text{S}$ NCs have often been obtained by using 1-DDT as sulfur sources without any coordinating agent or by using a non-coordinating agent 1-Octadecene (ODE) as a reaction medium. As these previous reports mentioned, the crystal phase and morphology of the products strongly depend on the choice of the surfactants and sulfur sources. However, there are few reports on the synthesis of Cu_{2-x}S NCs using different alkanethiols as sulfur sources.

In the present paper, a series of Cu_{2-x}S NCs have been synthesized by direct thermolysis of a mixed solution of copper acetylacetonate ($\text{Cu}(\text{acac})_2$) and different alkanethiols in a non-coordinating solvent, which avoids the pre-synthesis of any organometallic precursor and the injection of a toxic phosphine

agent. The effects of the alkyl chain length of alkanethiols on the crystal phase and morphology of the as-obtained Cu_{2-x}S have been studied in detail. When the alkanethiols with relatively short alkyl lengths, such as 1-octanethiol (1-OT) and 1-dodecanethiol (1-DDT), are used as sulfur sources, spherical $\text{Cu}_{1.94}\text{S}$ NCs can be obtained. In contrast, the crystal phase of the as-obtained products can be transformed from $\text{Cu}_{1.81}\text{S}$ to $\text{Cu}_{1.94}\text{S}$ by using 1-octadecanethiol (1-ODT) as a sulfur source at 200 °C for different reaction time, and the corresponding morphology changes from spheres to disks. When the reaction temperature is elevated to 240 °C, tetragonal $\text{Cu}_{1.81}\text{S}$ nanodisks have been obtained for different reaction time. Moreover, the effects of the thiol length on the NIR plasmonic absorption and the electrical properties of Cu_{2-x}S NCs have also been discussed.

Experimental

Materials

Copper (II) acetylacetonate ($\text{Cu}(\text{acac})_2$, $\geq 99\%$), 1-octanethiol (1-OT, $\geq 98\%$), 1-dodecanethiol (1-DDT, $\geq 98\%$) and 1-octadecanethiol (1-ODT, $\geq 97\%$) were purchased from Aladdin Chemical Reagent Co., Ltd., China. 1-octadecene (ODE, 90%) was purchased from J&K Chemical Ltd. Other solvents such as ethanol and acetone were commercially available products in analytical grade, which were purchased from Beijing Chemical Reagent, China. All the materials were used as purchased without further purification.

Synthesis of Cu_{2-x}S NCs

Table 1. Summary of synthetic parameters and the corresponding results

Samples	Sulfur Source	Temperature (°C)	Morphology	Crystal Phase
Sample A	1-OT	180	Nanospheres	$\text{Cu}_{1.94}\text{S}$
Sample B	1-OT	200	Nanospheres	$\text{Cu}_{1.94}\text{S}$
Sample C	1-DDT	200	Nanospheres	$\text{Cu}_{1.94}\text{S}$
Sample D	1-ODT	200	Nanospheres and Nanodisks	$\text{Cu}_{1.94}\text{S}$ and $\text{Cu}_{1.81}\text{S}$
Sample E	1-ODT	240	Nanodisks	$\text{Cu}_{1.81}\text{S}$

In a typical synthesis of Cu_{2-x}S NCs, $\text{Cu}(\text{acac})_2$ (3 mmol) and 1-DDT (2.86 mL, 12 mmol) were mixed with ODE (20 ml) in a 50ml four-necked flask. The oxygen in the reaction mixture was purged with N_2 glow for 20 min. Then the mixture was heated up slowly to 200 °C under magnetic stirring and the reaction temperature was kept 240 min. At the initial stage of the reaction process, the mixture became a yellow transparent solution. After several minutes, the solution became red, and finally it became a brown or black turbid solution. To monitor the size and shape evolution, the samples were collected from the mixture at every reaction stage. After the reaction was finished, the mixture was cooled to room temperature naturally. Afterwards, the absolute ethanol was added to precipitate the samples which were collected by centrifugation at 6000 rpm for 10 min, and then were purified by chloroform to remove any unwanted by-products. The precipitation and purification

processes were repeated three times, and the final products were dispersed in chloroform or dried under vacuum for next analyses. For the synthesis of the Cu_{2-x}S NCs using other alkanethiols with different alkyl length as sulfur sources, except reaction temperatures other reaction conditions remained the same. The detailed experimental conditions are summarized in Table.1, and the synthesis process of Cu_{2-x}S NCs using different alkanethiols is illustrated in Fig. 1.

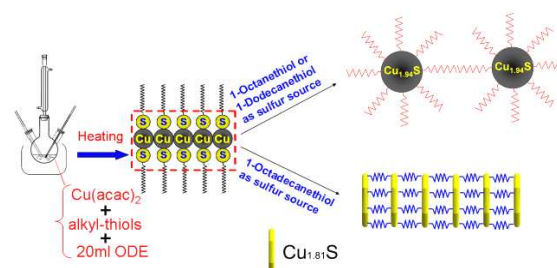


Fig. 1 Schematic illustration of the synthesis of different Cu_{2-x}S NCs using alkanethiols with different chain length.

Characterization

The crystal structure of the samples were measured using a Bruker D8 Discover X-ray Diffractometer with a $\text{CuK}\alpha$ radiation source ($\lambda=1.54056 \text{ \AA}$). Transmission electron microscopy (TEM) and high-resolution transmission electron microscopy (HRTEM) were performed using a Hitachi 7650 transmission electron microscope at an accelerating voltage of 100 kV and a JEM-2010 transmission electron microscope working at an accelerating voltage of 200 kV, respectively. The thermogravimetric analysis (TGA) was measured using a SDTA851E Thermogravimetric Analyzer. The UV-Vis absorption spectra were obtained by a Shimadzu-UV UV3101 spectrometer. Fourier transform infrared spectra (FTIR) were collected by a Nicolet-6700 spectrometer. The X-ray photoelectron spectroscopic (XPS) measurements were performed on an ESCALAB 250 spectrometer with a 300W Al $\text{K}\alpha$ radiation source. The current–voltage (I–V) characteristics of the device were measured by a Keithley 2410 source meter controlled by a computer. All the measurements were carried out at room temperature.

Results and discussions

As stated in previous reports that Cu-thiolate compounds could be formed through the reaction of copper salts and 1-DDT²³⁻²⁵. Herein, the reaction of $\text{Cu}(\text{acac})_2$ and alkanethiols with different alkyl lengths can also lead to the formation of different Cu-thiolate compounds, as demonstrated by the color change of the reaction mixture at the initial stage of the reaction (See Fig.S1 of ESI †). A similar color change has been observed in the heating-up process of the different reaction, and the color changes gradually from yellow to red, and then becomes dark-brown, which is attributed to a transition from the crystalline lamellar phase to a smectic-like phase²⁶. Interestingly, the reaction mixture becomes a gel when the as-collected samples are cooled down to room temperature, which

indicates the formation of the thiolate compounds with a layered structure based on the previous report^{23,24}. It is noted that the dark-brown sample using $C_8H_{17}SH$ as a sulfur source does not become a gel at room temperature (Fig. S1a, ESI †), but other two dark-brown samples using $C_{12}H_{25}SH$ and $C_{18}H_{37}SH$ are gel-like (Fig. S1b and c, ESI †), which may be in close association with the different chain length of the alkanethiols used in our work. This plausible conclusion can be demonstrated by the XRD patterns of the samples collected at the initial stage of the reaction (Fig. S2, ESI †). It can be seen that periodic arrangement appears in the low-angle diffraction peaks, which corresponds to the successive orders of diffraction from a layered thiolate compound. The interlayer distance calculated from the XRD patterns increases with the increasing alkyl lengths, indicating that the layered structure of Cu-thiolate compounds consists of stacked layers of Cu and S atoms separated by different alkyl chains²⁵⁻²⁷. The decomposition behaviors of different Cu-thiolate compounds have been studied by thermogravimetric analysis (TGA) (shown in Fig. S3, ESI †), and the initial decomposition temperature of the thiolate compounds is increased as the alkyl chain length of thiol increases, which indicates that the Cu-thiolate compound with a relatively short alkyl chain can decompose into small nuclei at a relatively low temperature. In contrast, the decomposition of the Cu-thiolate compound with a longer alkyl chain needs a higher temperature. Therefore, the synthesis of $Cu_{2-x}S$ NCs using alkanethiols with different alkyl length was performed at different reaction temperatures.

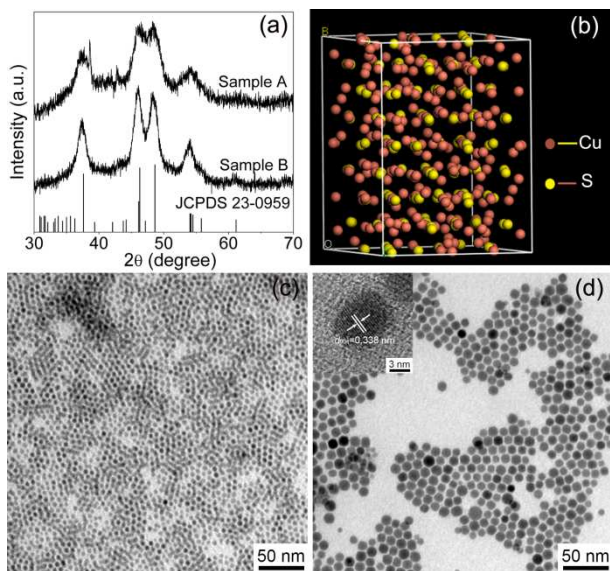


Fig. 2 (a) XRD patterns of sample A and sample B, and the vertical bars represent the standard diffraction peaks of monoclinic $Cu_{1.94}S$ phase (JCPDS No.23-0959), (b) Schematic model for the atomic arrangements of $Cu_{1.94}S$ crystals, and TEM images of (c) sample A and (d) sample B collected at 240 min.

Fig. 2 (a) shows the XRD patterns of sample A and sample B collected at 240 min, and there are four obvious diffraction peaks at 2 degree of 37.6° , 46.3° , 48.7° and 54.2° , which can be assigned to (8,0,4), (0,8,0), (12,0,4) and (8,8,0) planes of monoclinic $Cu_{1.94}S$ with P21/n (14) space group (JCPDS card 23-0959), which possesses a cationic deficiency structure and is

ascribed to djurleite phase in natural minerals. The corresponding schematic model for the atomic arrangements is shown in Fig.2 (b). As compared to sample A, the diffraction peaks of sample B becomes narrowed, which indicates that the particle size is increased with the increasing reaction temperature based on the Scherer equation. This deduction can be confirmed by the TEM results shown in Fig.2 (c) and (d). It can be observed that both the products exhibit a spherical shape with a uniform size distribution. As the reaction temperature is increased from 180 to 200 °C., the average size is increased from 5.5 ± 0.6 nm (sample A) to 10.8 ± 0.9 nm (sample B), and the corresponding size distribution histograms are given in Fig.S4 of ESI †. The HRTEM image of sample B shown in the inset of Fig. 2(d) reveals the well resolved lattice fringes, and the inter-fringe distance is measured to be about 0.338 nm ascribing to (004) plane of monoclinic $Cu_{1.94}S$ (JCPDS card 23-0959), which matches well with the XRD results.

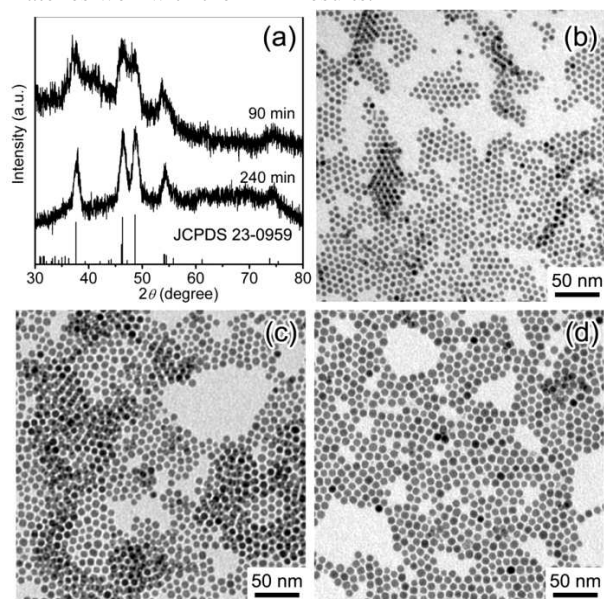


Fig. 3 (a) XRD patterns and TEM image of sample C obtained at different reaction time: (b) 90 min; (c) 120 min; (d) 240 min. The vertical bars shown in Fig.3(a) represent the standard diffraction peaks of monoclinic $Cu_{1.94}S$ phase (JCPDS No.23-0959)

The synthesis of $Cu_{1.94}S$ NCs using 1-DDT as a sulfur source has been studied extensively in previous reports²⁸⁻³⁰. Fig.3 shows the XRD patterns and TEM images of sample C collected at different reaction time. As shown in Fig.3(a), all the diffraction peaks of sample C obtained at 90 and 240 min confirm the formation of monoclinic $Cu_{1.94}S$ (JCPDS card 23-0959), and the diffraction peaks become narrowed as the reaction time is increased from 90 min to 240 min, indicating the particle size is increased with the prolonging of reaction time. The TEM images of sample C obtained at 90, 120 and 240 min are shown in Fig.3 (b)-(d), respectively and all the products remain spherical in shape with the average diameter of 6.1 ± 0.6 nm (90min), 6.3 ± 0.4 nm (120min) and 9.1 ± 1.0 nm (240 min), respectively (Fig.S5 of ESI †). It is noted that the average diameter of sample B obtained at 240 min is larger than

that of sample C at 240 min, which suggests that the nucleation and growth speed of the NCs is relatively faster in the case of the alkanethiols with a short alkyl length used as a sulfur source.

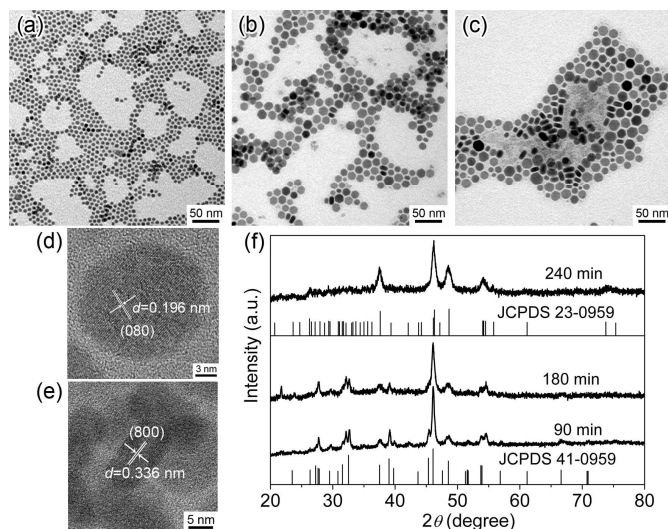


Fig. 4 TEM images of sample D for different reaction time: (a) 90 min; (b) 180 min; (c) 240 min; images of sample D obtained at 240 min: (d) the NDs lying flat on the substrate; (e) the NDs with surface perpendicular to the substrate; (f) XRD patterns of sample D for different reaction time, and the vertical bars represent the standard diffraction peaks of monoclinic $\text{Cu}_{1.94}\text{S}$ phase (JCPDS No.23-0959) and tetragonal $\text{Cu}_{1.81}\text{S}$ phase (JCPDS No.41-0959).

When 1-ODT was used as the sulfur source to prepare Cu_{2-x}S NCs, what happened to the morphology and crystal phase of the as-obtained products? Fig.4 shows the TEM images and XRD patterns of sample D obtained at different reaction time. As shown in Fig.4(a), the product obtained at 90 min exhibits a spherical shape with an average diameter of 6.0 ± 0.7 nm. When the reaction time is prolonged to 180 min, the morphology of the products transforms from disk-like to spherical shape, and most of the products are laid on their faces while only a small amount nanodisks are perpendicular to the substrate because the 1-ODT ligand passivation on the nanocrystal surface renders the disk surface hydrophobic (Fig. 4b).³¹ As the reaction time is prolonged from 120 min to 180 min, the diameter/thickness of the NDs changes from $13.0 \pm 1.3/ 8.1 \pm 0.9$ nm to $15.3 \pm 2.2/ 8.5 \pm 0.7$ nm while the disk shape is almost unchanged. The corresponding size distribution histograms of sample D obtained at different reaction time are given in Fig.S6 of ESI†. Careful inspection of the products obtained at 180 min shown in Fig.4 (c) suggests that the facet of the majority of the samples is hexagonal, which indicates that 1-ODT can direct the anisotropic growth of the Cu_{2-x}S NDs when it acts as the capping layer. Surprisingly, the XRD patterns of sample D shown in Fig.4 (f) indicate that all the diffraction peaks of sample D obtained at 90 min and 180 min match well with tetragonal $\text{Cu}_{1.81}\text{S}$ (JCPDS card 41-0959), which can be ascribed to digenite phase in natural minerals. To the best of

our knowledge, the Cu_{2-x}S NDs with such a phase have rarely been reported in previous report. As the reaction time is enhanced to 240 min, the crystal phase of sample D can be indexed as monoclinic $\text{Cu}_{1.94}\text{S}$, but the intensity of diffraction peak of (080) is increased significantly, which is very different with that of sample A and sample B. The result suggests that the priority growth direction is along the (080) facet, resulting in the formation of disks. To further study the crystal structure of the NDs, the HRTEM images of the product obtained at 240 min are given in Fig.4(d) and (e), respectively. Fig.4(d) shows the HRTEM image of $\text{Cu}_{1.94}\text{S}$ NDs lying flat on the substrate, and an obvious lattice fringe with inter planar spacing of 0.196 nm is observed, which corresponds to (080) plane of monoclinic $\text{Cu}_{1.94}\text{S}$ phase and is in agreement with the XRD result. In contrast, as shown in Fig.4(e), the inter planar spacing is measured to be about 0.336 nm for the NDs with surface oriented perpendicular to the substrate, which can be assigned to (800) plane. Both the XRD and TEM results that using 1-ODT as a sulfur source, the morphology of the Cu_{2-x}S NCs synthesized can be transformed from NSs to NDs, and the crystal phase is changed from tetragonal $\text{Cu}_{1.81}\text{S}$ to monoclinic $\text{Cu}_{1.94}\text{S}$. This change is attributed to the longer carbon chain length in 1-ODT³¹.

As stated in the TGA result of Fig.S3, the decomposition temperature is the highest for the thiolate compound formed by $\text{Cu}(\text{acac})_2$ and 1-ODT. As a result, the nucleation and growth slows down at the initial stage. With the reaction proceeding, enough energy has been provided to promote the formation of more active monomer species. Just as 1-OT and 1-DDT, 1-ODT acts not only as a sulfur source but also a capping ligand, which could be absorbed selectively onto the nanocrystal surface. However, -the alkyl chain length of ODT is relatively longer, which may facilitate the growth of (080) facets, lead to the anisotropic growth of NCs and thus produce the disk morphologies. On the other hand, the formation of tetragonal $\text{Cu}_{1.81}\text{S}$ phase may be the synergistic action of the different reduction abilities and the different binding to the NCs facets for different alkanethiols.

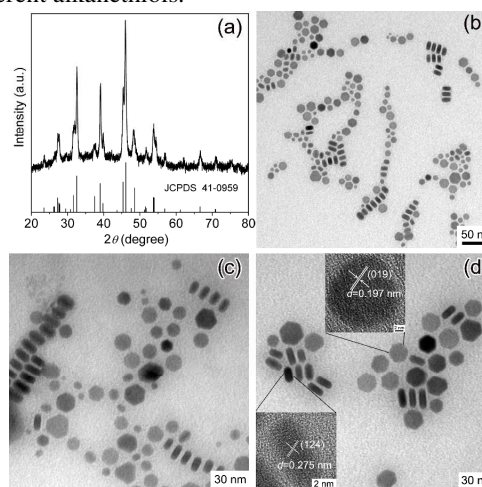


Fig. 5 (a) XRD patterns (bottom lines: standard diffraction lines of JCPDS card. 41-0959), and TEM images of sample E obtained at different reaction time: (b) 60 min, (c) 120 min and (d) 180 min, and the inset shows the HRTEM image of the NDs with the surface parallel or perpendicular to the substrate.

To further study the formation mechanism of the sample using 1-ODT as a sulfur source, the reaction temperature was enhanced to 240 °C, and the XRD and TEM images of sample E are given in Fig.5. All the diffraction peaks shown in Fig.5 (a) can be indexed to the tetragonal structure of $\text{Cu}_{1.81}\text{S}$ according to the standard pattern (JCPDS No. 41-0959), and no other diffraction peaks are observed, which indicates the formation of pure $\text{Cu}_{1.81}\text{S}$ phase with a tetragonal structure. Interestingly, the morphology of sample E for different reaction time is kept in disk shape (shown in Fig.5b-d), and the average diameter of sample E is increased from 11.3 ± 2.1 to 18.6 ± 2.7 nm as the reaction time is increased from 60 to 180 min while the thickness is kept similar. It is worthwhile to mention that the cross section of the as-obtained NDs changes from quasi-spherical to hexagonal with the increasing reaction time. To further confirm the formation of $\text{Cu}_{1.81}\text{S}$ disks, the HRTEM images of the NDs with the surface parallel or perpendicular to substrate have been given in the inset of Fig.5 (d). As compared to sample D, the NDs have been formed at 60 min when the reaction temperature is enhanced to 240 °C. As a matter of fact, higher temperature facilitates the decomposition of Cu-ODT intermediate complexes, which could provide more monomer species to promote the NCs nucleation and growth. Once the $\text{Cu}_{1.81}\text{S}$ nuclei were formed, the remaining monomer species could be deposited onto the surface of the nuclei to promote the progressive growth³². In addition, the free 1-ODT can be adsorbed onto the surface of the NCs to direct the NCs growth along the specific facet. To the best of our knowledge, the synthesis of $\text{Cu}_{1.81}\text{S}$ NDs has been rarely reported previously. However, the genuine reason for the formation of $\text{Cu}_{1.81}\text{S}$ disks remains unclear, and further study is on-going.

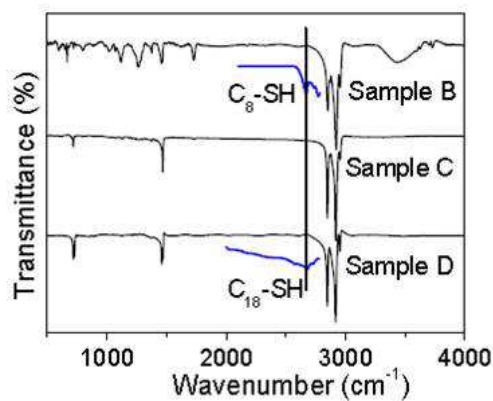


Fig. 6 FTIR spectra of Sample B-D, and the FT-IR spectra of pure 1-DT and 1-ODT are also given.

To explore the chemical bond of the surface of the Cu_{2-x}S NCs using different alkanethiols as sulfur sources, the FTIR spectra of sample B-D are depicted in Fig. 6. Two sharp peaks locating at 2921 and 2848 cm^{-1} are observed in the three samples, which correspond to the asymmetric methyl stretching and asymmetric methylene stretching modes, respectively. The decreasing intensity ratio of the two bands (I_{2917}/I_{2848}) indicates

that the alkyl chains become more orderly with the increase of alkyl chains due to the increasing Van Der Waals' interaction^{25, 27}. It is noted that the band at 2577 cm^{-1} induced by S-H stretching vibration disappear in sample B-D, which indicates the absence of free alkylthiol, and the formation of S-Cu bond.

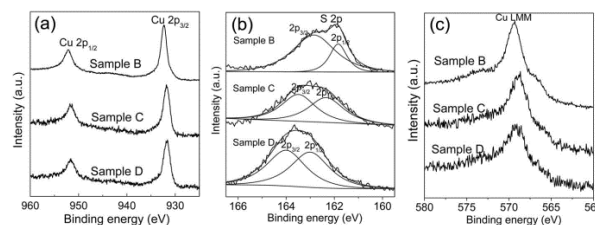


Fig. 7 XPS spectra of (a) Cu 2p, (b) S 2p and (c) AES spectra of Cu-LMM for sample B-D.

We employed XPS and Auger Electron Spectroscopy (AES) techniques to analyze the valence states and the composition of sample B-D. As shown in Fig.7(a), the Cu 2p_{3/2} and Cu 2p_{1/2} peaks of the three samples are symmetric and narrow, and the satellite peaks indicates that the monovalent copper related with Cu(II) have not been observed³³. Moreover, a slight shift of Cu 2p_{3/2} and Cu 2p_{1/2} peaks towards higher binding energy is observed as the alkyl length of the alkanethiols is increased, which can be attributed to the different binding energies of Cu with thiols for different alkanethiols. Considering the similarity of the binding energies for Cu(0) and Cu(I), the AES measurement for Cu LMM has been performed to prove the valence state of Cu in sample B-D. As shown in Fig.7(c), the Auger kinetic energies can be calculated to be in the range of 917.4-918 eV for sample B-D, which are in good agreement with the literature values²², and thus the monovalent copper in our samples has been further verified. The XPS results of S 2p for sample B-D shown in Fig.7(b) have been fitted into two peaks ascribing to 2p_{1/2} and 2p_{3/2} by using a spin-orbit separation of 1.1 eV, and the peaks shift to high binding energy with the increasing alkyl chains length of thiol molecules. Moreover, the intensity ratio of S 2p_{3/2} to S 2p_{1/2} decreases as the alkyl chains length is increased. As mentioned above, the Cu vacancies are present in our samples, which make the S ions in the lattice be partially oxidized, resulting the different oxidation states for S elements. Moreover, the different interaction between Cu and thiols may contribute to the shift of the S 2p peaks.³⁴⁻³⁷

Very recently, it has been reported that Cu_{2-x}S NCs exhibit strong LSPR absorption in NIR region, which originates from excess holes in the valence band due to Cu deficiencies^{13, 38, 39}. The LSPR absorption spectra have often been used to profile the stoichiometry and phase of copper chalcogenides NCs. Therefore, the UV-Vis-NIR absorption spectra have been employed to study the plasmonic behaviour of the products using different alkanethiols as sulfur sources, and we chose the sample B-D obtained at 90 min as investigation objects due to their spherical shape. Fig.8 shows the absorption spectra of sample B-D in chloroform. All samples exhibit a well-defined LSPR band, and an obvious blue-shift on the energy scale can

be observed in the LSPR band of sample D, which can be attributed to the increasing of Cu vacancies numbers.

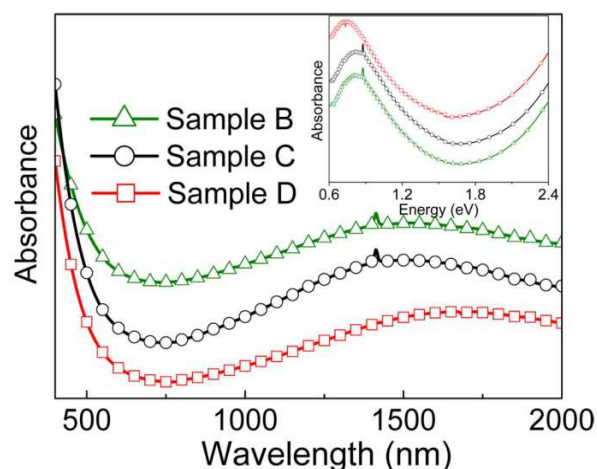


Fig. 8 LSPR spectra of sample B-D obtained at 90 min in chloroform, and the inset shows the absorption on the energy scale.

According to Mie-Drude model, the LSPRs frequency (ω_{sp}) can be expressed as follows:³⁸

$$\omega_{sp} = \sqrt{\frac{\omega_p^2}{1 + 2\varepsilon_m} - \gamma^2}$$

where ε_m represents the dielectric constant of the solvent (for chloroform, $\varepsilon_m = 4.8$ at 20 °C), ω_p is the bulk plasmon frequency and γ is the line width of the plasmon resonance band. Herein, the LSPRs frequency (ω_{sp}) of sample B-D is 0.81, 0.83 and 0.74 eV and the line width of the LSPRs band (γ) is 0.29, 0.25 and 0.17 eV, which was determined by fitting the NIR absorption band to a Gaussian function. As a result, ω_p is estimated to be about 2.80, 2.82 and 2.47 eV, respectively. The relationship between the carrier density (N_h) and the bulk plasmon frequency (ω_p) can be expressed by using the following equation:³⁸

$$\omega_p = \sqrt{\frac{N_h e^2}{\varepsilon_0 m_h}}$$

where e is the electron charge, ε_0 is free space permittivity and m_h is the hole effective mass (approximated as $0.8 m_0$, where m_0 is electron mass). From the above equation, N_h is estimated to be 4.61×10^{21} , 4.68×10^{21} and $3.59 \times 10^{21} \text{ cm}^{-3}$ for sample B, C and D, which are of the same order of magnitude as the value of copper chalcogenide films reported previously^{37,38}. Generally, the Copper vacancies are related to the stoichiometric of Cu_{2-x}S . According to the above XRD results, sample B and C obtained at 90 min have monoclinic $\text{Cu}_{1.94}\text{S}$ phase, however, the sample D belongs to tetragonal $\text{Cu}_{1.81}\text{S}$ phase, and the LSPR result is in accord with the XRD results.

The alkyl length has an important effect on the electrical properties of Cu_{2-x}S NCs due to the insulating alkyl groups on the surface of the NCs. The conductivity of the as-obtained

products using different alkanethiols as sulfur sources have been studied in ITO/ Cu_{2-x}S NCs/Al structure, and the corresponding *I-V* characteristics of sample B-D obtained at 60 min are given in Fig.S7 of ESI†. All the samples have the same molar concentration and the thickness of films is about 100 nm. It can be seen that the conductivity of the NCs decreases with the increase of alkyl length due to its larger inter-particle spacing and high resistance. The result may direct the potential applications of Cu_{2-x}S NCs in electricity devices in the future.

Conclusions

In summary, we have successfully synthesized Cu_{2-x}S NCs with different morphologies and crystal phases by controlling the alkyl lengths of alkanethiols and reaction temperatures through a simple one-pot method. When 1-OT and 1-DDT have been chosen as sulfur sources, monodispersed djurleite $\text{Cu}_{1.94}\text{S}$ nanospheres with monoclinic structures have been obtained at relatively low temperature, such as 200 °C. As the alkanethiol is changed to 1-ODT, the morphology is changed from nanospheres to nanodisks with the reaction time increasing. Interestingly, the crystal phase transforms from tetragonal $\text{Cu}_{1.81}\text{S}$ to monoclinic $\text{Cu}_{1.94}\text{S}$ with the reaction time prolonging at 200 °C. When the reaction temperature is increased to 240 °C, the disk-shaped $\text{Cu}_{1.81}\text{S}$ can be successfully obtained. Different characterization techniques including FTIR, XPS, plasmonic absorption spectra have been used to study the effects of different alkanethiols as sulfur sources on the crystal phase and chemical composition of the as-obtained products. The LSPR wavelength of the different Cu_{2-x}S NCs can be tuned due to the size, morphology and crystal phase change. The study about the Cu_{2-x}S thin films shows a strong dependence on the ligand length of the different Cu_{2-x}S NCs, which foreshows a promise application in the next-generation optoelectronic devices in the near future.

Acknowledgements

This work was partly supported by the Fundamental Research Funds for the Central Universities (2014JBZ010), National Natural Science Foundation of China (No.61108063, No. 61205180), and the National Natural Science Foundation for Distinguished Young Scholars of China (No. 61125505), and Natural Science Foundation of Hebei Province (Grants No. E2012201087). We also appreciate the financial support from the Program for Top Young Talents of Hebei Province.

Notes and references

^aKey Laboratory of Luminescence and Optical Information, Ministry of Education, School of Science, Beijing Jiao Tong University, Beijing 100044, China. E-mail: awtang@bjtu.edu.cn.

^bHebei Key Laboratory of Optic-electronic Information and Materials, College of Physics Science and Technology, Hebei University, Baoding 071002, PR China. E-mail: fteng@bjtu.edu.cn.

*Aiwei Tang, E-mail: awtang@bjtu.edu.cn; Tel +86 10 51683627.

FengTeng, E-mail: fteng@bjtu.edu.cn (F. T.).

Notes The authors declare no competing financial interest

- 1 D. V. Talapin, J. S. Lee, M. V. Kovalenko, E. V. Shevchenko, *Chem. Rev.*, 2010, **110**, 389-458.
- 2 Y. L. Zhou, Z. N. Zhu, W. X. Huang, W. J. Liu, S. J. Wu, X. F. Liu, Y. Gao, W. Zhang, Z. Y. Tang, *Angew. Chem. Int. Ed.* 2011, **50**, 11456-11459.
- 3 L. Qian, J. H. Yang, R. J. Zhou, A. W. Tang, Y. Zheng, T. K. Tseng, D. Bera, J. G. Xue, P. H. Holloway, *J. Mater. Chem.* 2011, **21**, 3814-3817.
- 4 W. Han, L. X. Yi, N. Zhao, A. W. Tang, M. Y. Gao, Z. Y. Tang, *J. Am. Chem. Soc.* 2008, **130**(39), 13152-13161.
- 5 X. Q. Zhou, A. C. Soldat, and C. Lind, *RSC Adv.*, 2014, **4**, 717-726.
- 6 W. H. Li, R. Zamani, P. R. Gil, B. Pelaz, M. Ibáñez, D. Cadavid, A. Shavel, R. A. Zlvarez-Puebla, W. J. Parak, J. Arbiol, and A. Cabot, *J. Am. Chem. Soc.*, 2013, **135**, 7098-7101.
- 7 Y. Xie, A. Riedinger, M. Prato, A. Casu, A. Genovese, P. Guardia, S. Sottini, C. Sangregorio, K. Miszta, S. Ghosh, T. Pellegrino and L. Manna, *J. Am. Chem. Soc.*, 2013, **135**, 17630-17637.
- 8 G. Manna, R. Bose, and N. Pradhan, *Angew. Chem. Int. Ed.*, 2013, **52**, 6762-6766.
- 9 Y. Z. Wei, G. S. Wang, Y. Wu, Y. H. Yue, J. T. Wu, C. Lu, L. Guo, *J. Mater. Chem. A*, 2014, **2**, 5516-5524.
- 10 L. L. Quan, W. P. Li, L. Q. Zhu, X. W. Chang and H. C. Liu, *RSC Adv.*, 2014, **4**, 32214-32220.
- 11 Y. X. Zhao, H. C. Pan, Y. B. Lou, X. F. Qiu, J. J. Zhu and C. Burda, *J. Am. Chem. Soc.*, 2009, **131**, 4253-4261.
- 12 C. M. Hessel, V. P. Pattani, M. Rasch, M. G. Panthani, B. Koo, J. W. Tunnell and B. A. Korgel, *Nano. Lett.*, 2011, **11**, 2560-2566.
- 13 L. G. Liu, H. Z. Zhong, Z. L. Bai, T. Zhang, W. P. Fu, L. J. Shi, H. Y. Xie, L. G. Deng and B. S. Zou, *Chem. Mater.*, 2013, **25**, 4828-4834.
- 14 S. Lv, H. Suo, X. Zhao, C. X. Wang, T. L. Zhou, S. Y. Jing, Y. N. Xu and C. Zhao, *J. Alloy. Compound.*, 2009, **479**, L43-L46.
- 15 S. Gorai, D. Ganguli, S. Chaudhuri, *Cryst. Growth. Des.*, 2005, **5**, 875-16 L. Chen, Y. B. Chen, L. M. Wu, *J. Am. Chem. Soc.*, 2004, **126**, 16334.
- 17 M. D. Regulacio, C. Ye, S. H. Lim, M. Bosman, L. Polavarapu, W. L. Koh, J. Zhang, Q. H. Xu, and M. Y. Han, *J. Am. Chem. Soc.*, 2011, **133**, 2052-2055.
- 18 Z. B. Zhuang, Q. Peng, B. C. Zhang and Y. D. Li, *J. Am. Chem. Soc.*, 2008, **130**, 10482-10483.
- 19 M. B. Sigman, A. Ghezelbash, T. Hanrath, A. E. Saunders, F. Lee, and B. A. Korgel, *J. Am. Chem. Soc.*, 2003, **125**, 16050-16057.
- 20 M. Kruszynska, H. Borchert, A. Bachmatiuk, M. H. Rummeli, B. Büchner, J. Parisi and J. Kolny-Olesiak, *ACS Nano.*, 2012, **6**, 5889-5896.
- 21 N. J. Freymeyer, P. D. Cunningham, E. C. Jones, B. J. Golden, A. M. Wiltrout and K. E. Plass, *Cryst. Growth. Des.*, 2013, **13**, 4059-4065.
- 22 A. W. Tang, S. C. Qu, K. Li, Y. B. Hou, F. Teng, J. Cao, Y. S. Wang and Z. G. Wang, *Nanotechnology.*, 2010, **21**, 285602-1-9.
- 23 H. T. Zhang, G. Wu, X. H. Chen, *Langmuir.*, 2005, **21**, 4281-4282.
- 24 L. Chen, Y. B. Chen, L. M. Wu, *J. Am. Chem. Soc.*, 2004, **126**, 16334-16335.
- 25 R. G. Snyder, H. L. Strauss and C. A. Elliger, *J. Phys. Chem.*, 1982, **86**, 5145-5150.
- 26 M. J. Baena, P. Espinet, M. C. Lequerica, A. M. Levelut, *J. Am. Chem. Soc.*, 1992, **114**, 4182-4185.
- 27 M. D. Porter, T. B. Bright, D. L. Allara and C. E. D. Chidsey, *J. Am. Chem. Soc.*, 1987, **109**, 3559-3568.
- 28 S. Jun, E. Jang, and Y. Chung, *Nanotechnology.*, 2006, **17**, 4806-4810.
- 29 V. F. Puentes, D. Zanchet, C. K. Erdonmez, and A. P. Alivisatos, *J. Am. Chem. Soc.*, 2002, **124**, 12874-12880.
- 30 X. M. Li, H. B. Shen, S. Li, J. Z. Niu, H. Z. Wang and L. S. Li, *J. Mater. Chem.*, 2010, **20**, 923-928.
- 31 W. Bryks, M. Wette, N. Velez, S. W. Hsu, and A. R. Tao, *J. Am. Chem. Soc.* 2014, **136**, 6175-6178.
- 32 Y. Wang, Y. X. Hu, Q. Zhang, J. P. Ge, Z. D. Lu, Y. B. Hou and Y. D. Yin, *Inorg. Chem.*, 2010, **49**, 6601-6608.
- 33 W. L. Sun, J. Xia, Y. C. Shan, *Chem. Eng. J.*, 2014, **250**, 119-127.
- 34 H. Z. Zhong, Y. Zhou, M. F. Ye, Y. J. He, J. P. Ye, C. He, C. H. Yang and Y. F. Li, *Chem. Mater.*, 2008, **20**, 6434-6443.
- 35 Z. Mekhalif, F. Laffineur, N. Couturier and J. Delhalle, *Langmuir.*, 2003, **19**, 637-645.
- 36 C. H. Kuo, Y. T. Chu, Y. F. Song, and M. H. Huang, *Adv. Funct. Mater.*, 2011, **21**, 792-797.
- 37 Y. Xie, A. Riedinger, M. Prato, A. Casu, A. Genovese, P. Guardia, S. Sottini, C. Sangregorio, K. Miszta, S. Ghosh, T. Pellegrino, and L. Manna, *J. Am. Chem. Soc.*, 2013, **135**, 17630-17637.
- 38 J. M. Luther, P. K. Jain, T. Ewers and A. P. Alivisatos, *Nat. Mater.*, 2011, **10**, 361-366.
- 39 H. H. Ye, A. W. Tang, L. M. Huang, Y. Wang, C. H. Yang, Y. B. Hou, H. S. Peng, F. J. Zhang and F. Teng, *Langmuir.*, 2013, **29**, 8728-8735.